Low-energy excitations in yttria-stabilized zirconia

F. J. Walker and A. C. Anderson
Department of Physics and Materials Research Laboratory, 104 South Goodwin, University of Illinois at Urbana-Champaign, Urbana, Illinois 61801
(Received 22 November 1983)

Measurements of the specific heat, thermal conductivity, dielectric constant and thermal expansion of the single-crystal fast-ion conductor $(ZrO_2)_{1-x}(Y_2O_3)_x$ with $x=0.10$, 0.16, and 0.18 exhibit behavior similar to that observed in amorphous solids and attributed to two-level states. The data can be fitted by the phenomenological tunneling states model, but at the expense of a more complex spectrum of two-level-state equilibration times than has generally been used for amorphous solids. The possible relationship of the two-level states with known defects is explored and found to be unsatisfactory.

I. INTRODUCTION

The thermal properties of pure, crystalline dielectric materials at temperatures $T \lesssim 1$ K exhibit Debye behavior. The specific heat is due entirely to the acoustic-phonon excitations which produce a cubic temperature dependence with a magnitude dependent on the elastic properties of the crystal. Thermal transport is due to the acoustic phonons which have mean free paths determined by the size of the sample. Thus the thermal conductance has a cubic temperature dependence and a magnitude that is sample-size dependent. Debye thermal properties should also be expected in glasses below 1 K since glasses, similar to crystals, should respond as a continuum with respect to the acoustic phonons. From experimental data, however, it is seen that glasses have additional excitations which contribute an excess specific heat and extra sources for phonon scattering.[1] The excess specific heat and the phonon scattering strength have roughly the same magnitude for nearly all amorphous materials, independent of composition.

In order to reproduce the temperature dependences of the thermal conductivity and specific heat in glasses, Anderson, Halperin, and Varma[2] and Phillips[3] (AHVP) introduced quantum-mechanical two-level states (TLS) with a broad distribution in energy splittings. These TLS serve both to enhance the specific heat and, through coupling to strain fields, scatter phonons. As a source of the TLS, AHVP proposed tunneling by a single atom or a group of atoms through the barrier of a double-well potential shown in Fig. 1. The required broad energy distribution of TLS is thought to arise from a broad distribution of double-well parameters of TLS residing in random local environments. The model has predicted properties not seen in pure crystals.[1] But, without knowledge of the microscopic tunneler, the AHVP model remains phenomenological and provides no explanation for the similar magnitudes of the thermal conductivity and specific heat of many types of glasses.

Tunneling states have been observed in defective crystalline solids through specific-heat and thermal-conductivity measurements at $T < 1$ K. For KCl containing a small concentration of Li ions, a Schottky peak is seen in the specific heat and a resonant scattering is observed in the thermal conductivity.[4] This behavior has been attributed to tunneling of the Li^+ ions. When Li^+ is substituted for K^+ on the cation sublattice, the small size of the lithium ion enables eight equivalent off-site positions to become energetically favorable. The Li^+ tunnels between these eight positions.

Low-energy excitations were also observed in the superionic conductor hollandite through the measurement of the specific heat[5] at $T < 10$ K. Hollandite is a one-dimensional K^+-ion conductor, where the K^+ ions are modeled as occupying the wells of a one-dimensional sinusoidal potential. When interactions between the K^+ ions are included, different configurations of K^+ ions in the wells have energy differences of approximately 1 K, giving rise to the observed specific heat anomaly near 1 K.

In the preceding two examples, microscopic knowledge of the defects existing in the material was crucial to understanding the source of the low-energy excitations. The lattice structure found in KCl:Li or hollandite is missing in glasses, making it difficult to identify the microscopic source of the excitations. Additional under-

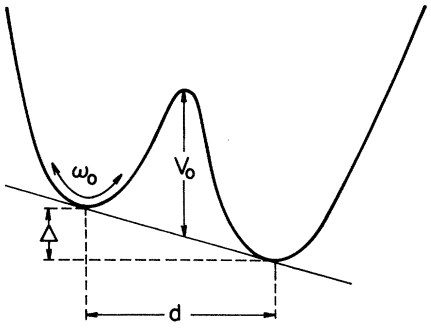

FIG. 1. Potential energy, versus a tunneling coordinate, used to approximate the TLS found in disordered solids. The angular resonant frequency for a single well is ω_0.

standing of TLS excitations may be possible through further study of materials which have well-defined lattices but exhibit "glassy" properties at low temperatures. A number of these crystals have been found[6,7] through the measurement of thermal conductivity, specific heat, and dielectric susceptibility for $T < 1$ K.

Of these glassy crystals, the M β-aluminas are well characterized.[8] Similar to KCl:Li and hollandite, the crystalline structure of M β-alumina is known. The cations M (Li, Na, Ag, or K) occupy planes which lie between plates of crystalline alumina. The planes contain a stoichiometric excess of M ions, thus giving rise to disorder in the cation planes. It is thought that, from this disorder, the observed glassy properties arise.[9] However, an attempt to reduce disorder by improving the stoichiometry did not alter the low-temperature dielectric response.[10]

The superionic conductor ZrO_2 doped with Y_2O_3 is another crystal which possesses some degree of disorder and which displays glassy properties[6] arising from defects introduced by the Y_2O_3. An important feature of this system is that inexpensive, large single crystals are available from the jewelry industry. Also, the density of defects that give rise to the TLS can be varied by changing the Y_2O_3 content. In the following, we report measurements of thermal conductivity, specific heat, dielectric constant, and thermal-expansion coefficient for single-crystal samples of ZrO_2 containing 10, 16, and 18 mol% Y_2O_3. The results are compared with the AHVP tunneling-state model. This model can account for the observed behavior, but only through the use of an extended array of adjustable constants.

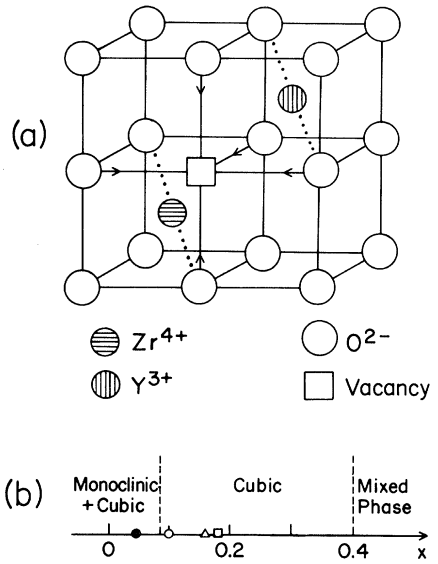

FIG. 2. (a) Defective cubic fluorite structure of stabilized ZrO_2:Y_2O_3. The arrows represent the collapse of the oxygens toward the vacancy. (b) Room-temperature phases of $(ZrO_2)_{1-x}(Y_2O_3)_x$ as a function of Y_2O_3 concentration x. The solid circle represents the composition of the ceramic sample measured in Ref. 6. The open symbols represent samples used for the present work. The same symbols are used in Figs. 3 and 10.

II. SAMPLE DESCRIPTION AND MEASUREMENT TECHNIQUE

At room temperature, ZrO_2 has a monoclinic crystal structure. Above 2370 °C, ZrO_2 possesses a cubic fluorite structure. When ZrO_2 is doped with Y_2O_3, the resultant solid solution may have a mixture of phases or a defective single phase. For Y_2O_3 concentrations of 9 to 40 mol% Y_2O_3, the ZrO_2:Y_2O_3 solid solution is stabilized into a cubic fluorite structure, Fig. 2, as deduced from a combination of diffuse x-ray-scattering,[11] neutron-scattering[12] and Raman scattering data.[13] The basic cubic fluorite structure contains a face-centered-cubic cation sublattice with the yttrium cation occupying substitutional sites. The oxygen sublattice is simple cubic with oxygen vacancies being introduced as the result of the $+3$ charge of yttrium as compared to the $+4$ charge of zirconium. Thus, for every two yttrium ions, charge compensation requires one oxygen vacancy. At high temperatures, as the solid solution cools from the melt, the oxygen vacancies are highly mobile. Coulombic interactions between the vacancies and yttrium cations tend to pair the vacancies and yttrium cations so that, at room temperature, the oxygen vacancy has at least one yttrium cation associated with it as a nearest neighbor.[14,15] Knowledge about ZrO_2:Y_2O_3 stems mainly from interest in its oxygen-conducting properties.

Three single-crystal samples[16] contained quoted Y_2O_3 concentrations of 10, 16, and 18 mol%. The position of each of the samples in the room-temperature phase diagram is shown in Fig. 2(b). The 10- and 16-mol% Y_2O_3 samples were colorless and clear of visible defects, but the 18-mol% sample had a yellowish tinge.[17] The Y_2O_3 concentrations of the three samples were estimated using three methods: the lattice parameter, which has been measured by many workers as a function of concentration,[18] the mass density, which also has been characterized,[19] and neutron activation.[20] The lattice parameters for these samples were measured using powder diffractometry. The results are listed in Table I. For the mass

TABLE I. Estimates of yttrium content in samples of $(ZrO_2)_{1-x}(Y_2O_3)_x$.

Sample	Vendor (Ref. 16)	Neutron activation	Density	Adjusted density	X ray
$x=0.10$	0.094	0.09 ±0.007	0.09	0.108	0.106±0.002
$x=0.16$	0.16	0.101±0.007	0.12	0.16	0.159±0.002
$x=0.18$	0.18	0.126±0.011	0.16	0.19	0.179±0.002

densities, it is not known whether the samples measured in Ref. 19 contained the ≈ 1 wt. % Hf that our samples contained (Table II). If Hf was present, the resulting yttrium content for our samples is that listed under the column "adjusted density" in Table I. We will refer to the three crystals as $(ZrO_2)_{1-x}(Y_2O_3)_x$ with $x = 0.10$, 0.16, or 0.18.

An indication of other impurities present in the samples may be obtained from the quoted impurity content of the ZrO_2 and Y_2O_3 starting materials; see Table II. The crystals were grown by the skull method in which the mixture of ZrO_2 and Y_2O_3 powder is melted by induction heating of metallic Zr at the center of the mix while the sides are cooled. An advantage of this method is that the melt comes into contact only with its own starting powder, thus reducing the influx of additional impurities.

Thermal-conductivity samples were made by cutting rectangular bars along the long axis ($\approx\langle 110\rangle$) of the boules using a diamond wafering saw. The surfaces left by the saw were rough and were not treated further. A two-heater method was used to measure the thermal conductivities of all three samples. In this method one thermometer is placed at the free end of the sample. A temperature difference is measured by switching heater power from one heater to the other. Samples for dielectric measurements were cut with thicknesses of ≈ 0.025 cm. The electrodes were silver paint applied to both sides of the sample with areas of ≈ 2.0 cm^2. The samples were mounted, thermally and electrically, as discussed previously.[21] Thermal-expansion measurements were made on a $x = 0.16$ rod cut from the long edge of the thermal-conductivity sample. The sample was mounted in a dilatometer described previously.[22]

We discuss the specific-heat measurement in greater detail so as to assure the reader that the anomalous response to be reported below is in fact intrinsic to the ZrO_2:Y_2O_3. Each sample, roughly a 1-cm cube, was rigidly clamped between copper plates. The plates were mechanically and thermally attached to the refrigerator. Thermal isolation between sample and copper plates was provided by dry, 0.02-cm-thick plates of sapphire.[23] The heater was fashioned from Pt-W wire distributed over one face of the cube, and attached with GE7031 varnish. The electrical leads were 0.005-cm-diam superconducting NbTi wire.[24] The carbon-chip thermometer was placed on the opposite face of the cube. The thermometer was ground from a 100-Ω Matsushita carbon-composition resistor,[25] and the leads were PbSn film vapor deposited on Mylar.[26] All leads were stretched taut to reduce vibrational heat influxes. Addenda contributed less than 3% to the measured heat capacity at temperatures below 1 K. In obtaining a specific-heat measurement, current pulses of 0.01 sec duration were applied to the heater, and the output of the resistance bridge was recorded and averaged in a signal-averaging computer.[26]

TABLE II. Impurity content of $(ZrO_2)_{1-x}(Y_2O_3)_x$ samples. (a) A typical analysis for the starting Y_2O_3 powder (Ref. 16). (b) Hafnium content deduced from neutron activation (Ref. 20). The starting ZrO_2 powder contained less than 0.006 wt. % Fe_2O_3 (Ref. 16).

(a)

Element	Content (ppm)
Tb	25
Yb	5.5
Gd	3.4
Ho	<0.1
Other lanthanides	<1.7
Fe	<10

(b)

x	Hf (wt. %)
0.10	1.03
0.16	0.63
0.18	0.88

III. RESULTS

All measurements on cubic ZrO_2:Y_2O_3 exhibit behavior similar to that found in amorphous solids and certain other disordered crystals.

A. Thermal conductivity

The thermal-conductivity data are displayed in Fig. 3. Data from a ceramic sample[6] [see Fig. 2(b)] are included for comparison. In the ceramic sample, phonon scattering from voids reduces the thermal conductivity. A similar reduction probably occurs at the lowest temperature for the present single-crystal samples due to scattering from

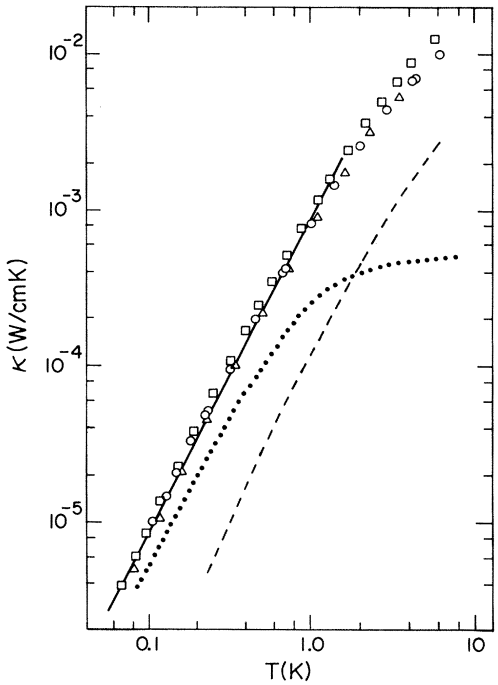

FIG. 3. Thermal conductivity of ZrO_2:Y_2O_3. ○, $x = 0.10$; △, $x = 0.16$; □, $x = 0.18$. The dashed line represents ceramic $(ZrO_2)_{0.955}(Y_2O_3)_{0.045}$ from Ref. 6, the dotted line is for an amorphous polymer (Ref. 38), and the solid line is computed from the AHVP model.

sample surfaces, but this would only be a 10% effect near 0.06 K.

The approximate T^2 behavior of Fig. 3 is typical of glassy materials, as is the magnitude of the conductivity κ. A roughly temperature-independent region, or "plateau," found in glasses near 1—10 K is not evident in Fig. 3, but measurements to higher temperatures on the ceramic[6] suggested the presence of a plateau near 20 K.

In the dominant-phonon approximation, κ may in general be written

$$\kappa = 4.08 \times 10^{10} T^3 l / v^2 \ (\mathrm{W/cm\,K}), \quad (1)$$

where l is the phonon mean free path and v is an average phonon velocity. Since κ (Fig. 3) and v (Ref. 27) are nearly independent of Y_2O_3 content, l is also independent of Y_2O_3 content.

B. Thermal expansion

Data for the thermal-expansion coefficient α are shown in Fig. 4. The coefficient approaches a linear temperature dependence at $T < 2$ K. The Grüneisen parameter Γ, defined as

$$\Gamma = 3\alpha B / C \ , \quad (2)$$

where B is the bulk modulus and C the specific heat, is plotted in Fig. 5. Figure 5 includes, for comparison, the Grüneisen parameters for two other crystals which exhibit glassy behavior, namely Na β-alumina[28] and KBr:KCN.[29]

C. Dielectric response

Figure 6 displays the real component ϵ' of the dielectric constant of $(ZrO_2)_{0.84}(Y_2O_3)_{0.16}$ as a function of frequency ν. A minimum near 0.1 K (for frequencies of 10^2—10^5 Hz) which scales as $\nu^{1/3}$ is typical of glassy solids.[30] Figure 7 shows the dependence on Y_2O_3 content. The position of the minimum is nearly independent of Y_2O_3 content, but the slope of ϵ versus T at lower temperatures appears to be weakly dependent on Y_2O_3 content. The loss component ϵ'' of the dielectric constant could not be measured with precision, but is shown qualitatively in Fig. 8.

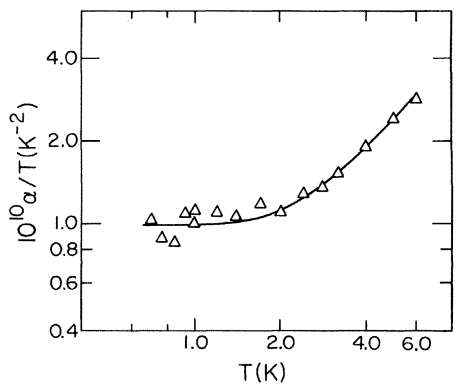

FIG. 4. Linear thermal-expansion coefficient, divided by temperature, of $(ZrO_2)_{0.84}(Y_2O_3)_{0.16}$. The solid line was used to compute the Grüneisen parameter shown in Fig. 5.

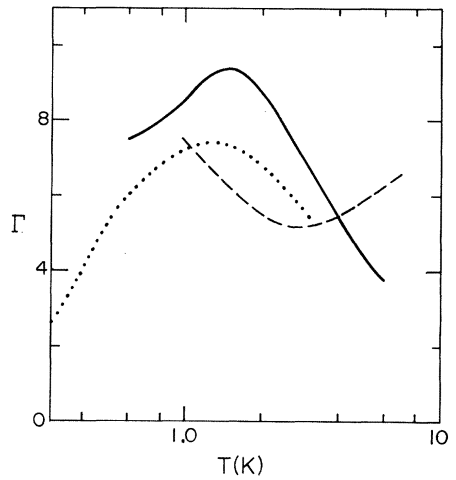

FIG. 5. Grüneisen parameter Γ for $(ZrO_2)_{0.84}(Y_2O_3)_{0.16}$ is shown by the solid line. Also shown are the Grüneisen parameters for Na β-alumina (dashed line) (Ref. 28), and KBr doped with KCN (dotted line) (Ref. 29). The Γ attributed to phonons is ≈ 2.

The temperature dependence of ϵ'' is similar to that of crystalline Na β-alumina.[21]

D. Specific heat

The specific-heat results were not typical of those seen for glasses or pure crystals obtained on a similar time scale. Normally, after the heat pulse is applied to the heater at time $t = 0$ s and the temperature rises, an exponential decay follows in T versus t. The time constant τ_{ext} of this decay is determined by the total heat capacity C_{tot} and the thermal impedance Z between the sample and the refrigerator,

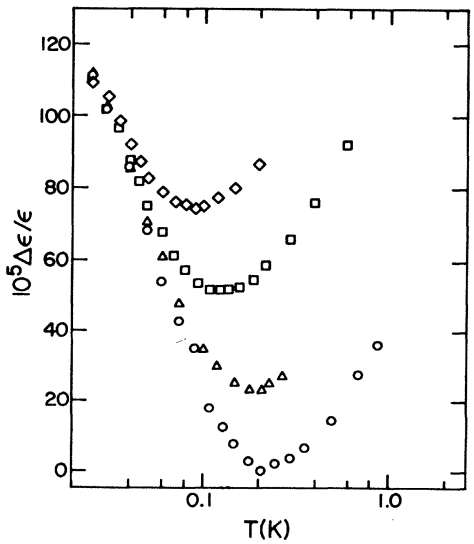

FIG. 6. Dielectric constant for $(ZrO_2)_{0.84}(Y_2O_3)_{0.16}$ scaled to coincide at low temperatures. ◇, 10^3 Hz; □, 3×10^3 Hz; △, 10^4 Hz; ○, 2×10^4 Hz.

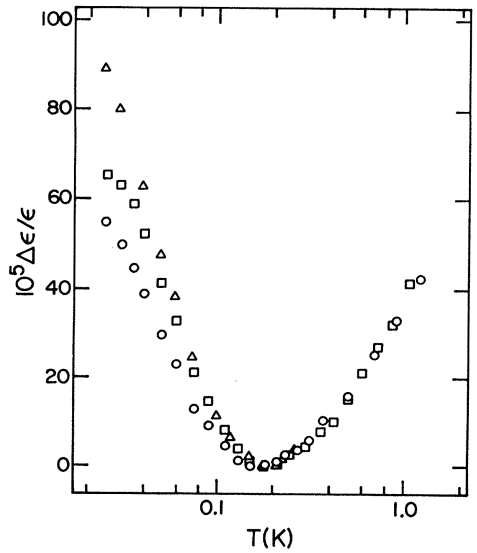

FIG. 7. Comparison of the dielectric constants for the three samples at 10^4 Hz. ○, $x=0.10$; △, $x=0.16$; □, $x=0.18$.

$$\tau_{\text{ext}} \approx ZC_{\text{tot}} , \tag{3}$$

with $\tau_{\text{ext}} \approx 15$ s near 0.25 K. Instead of this behavior, for $T < 1$ K, the temperature overshot the expected exponential decay and only after long times approached an exponential time dependence as shown in Fig. 9. A similar behavior has been observed for amorphous solids,[31] but on a much shorter time scale.

This overshoot can be understood if excitations exist in the material which have relaxation times on the order of seconds. Conceptually, the thermal impedance Z in Eq. (3) is infinite so that none of the heat injected by the heater leaks out of the sample during the time of the measurement. At short times after the heat pulse, excitations having long relaxation times have not equilibrated, so much of the energy is in the phonons plus those excitations which do relax quickly. The carbon-resistance thermometer records only the phonon temperature. As phonon energy is given up to the long-relaxation-time excitations, the phonon temperature drops until equilibrium is established within the sample. It is this final equilibrium temperature which is used to compute the total specific heat of the sample.

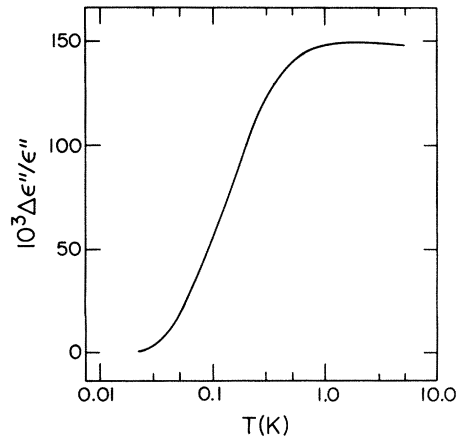

FIG. 8. Temperature dependence of the loss component ϵ'' of the dielectric constant at 10^4 Hz for $(ZrO_2)_{0.90}(Y_2O_3)_{0.10}$. Similar curves were obtained for $x=0.16$ and 0.18.

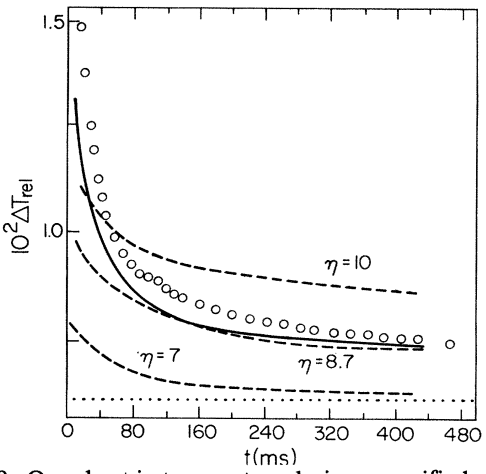

FIG. 9. Overshoot in temperature during a specific-heat measurement on $(ZrO_2)_{0.84}(Y_2O_3)_{0.16}$ at $T=0.25$ K. The dotted line represents the exponential dependence which would occur if the sample had a short internal equilibration time. The data (○) initially fall well above this line. The data have been divided by the temperature rise expected if only phonons had contributed to the specific heat, indicating that the observed specific heat is roughly a factor of 100 larger than the Debye contribution. As discussed in Sec. IV, the dashed line represents calculations, using standard levels only (Fig. 11), in which η of Eq. (7) was varied as indicated while the product $\bar{P}\eta$ was kept fixed. The solid line includes the anomalous TLS of Fig. 11, using the parameters listed in Table III.

When Z is finite, internal equilibrium may never be established. An approximation is obtained by extrapolating to $t=0$ s the nearly exponential decay observed at the longest times. This approximate value of the total specific heat is shown in Fig. 10. Internal equilibration was a problem only for $T < 1$ K.

In order to measure more of the excitations having long relaxation times, τ_{ext} needs to be increased by increasing Z of Eq. (3). For large Z, however, any spurious heat leak to the sample will elevate the sample temperature above the refrigerator temperature, preventing *in situ* calibration of the carbon thermometer. Indeed, a spurious heat leak prevented calibration of the thermometer below 0.2 K. This heat leak was unusually large to be due to vibration of leads, a typical source of spurious heat influx. Also, special care was taken to mount the sample rigidly and to stretch the electrical leads taut so that vibrational heating would be kept to a minimum. It is possible that the observed heat leak was due to excitations relaxing so slowly that equilibrium was not achieved for days. In brief, both the temperature overshoot and the residual heat leak suggest the presence of excitations having a broad spectrum of thermal equilibration times.

Another potential problem in the specific-heat data is

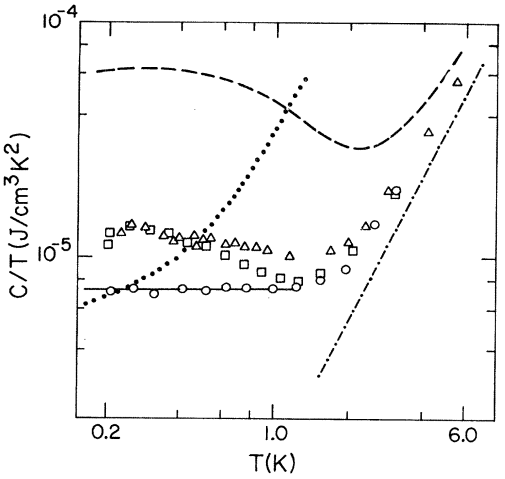

FIG. 10. Total specific heat of $(ZrO_2)_{1-x}(Y_2O_3)_x$, divided by temperature. ○, $x=0.10$; △, $x=0.16$; □, $x=0.18$. The dashed line is for $x=0.045$, ceramic sample, Ref. 6. The dotted-dashed line is the Debye specific heat expected from the measured room-temperature sound velocities. For comparison the specific heat of an amorphous polymer is shown by the dotted line (Ref. 38). The solid line is computed from the AHVP model.

the contribution from impurities listed in Table II. Neutron-activation analyses on the samples showed hafnium to be present with concentrations ranging from 0.63 to 1.03 wt.%. In addition, a "typical" analysis, supplied by the vendor,[16] of the Y_2O_3 powder used to make the cubic zirconia indicates 25 wt. ppm terbium. The possibility of these two impurities contributing significantly to the specific heat can be examined.

Hafnium has been cited before as contributing to the specific heat of a 4.5-mol% Y_2O_3 ceramic sample through its nuclear electric quadrupole moment.[32,33] An estimate[34] of the nuclear energy splittings gives ≈ 0.002 K. Hence, in our temperature range, we should see only the T^{-2} portion of the resulting Schottky peak. A rough estimate of the magnitude of this contribution suggests only an $\approx 3\%$ contribution to the specific heat at the lowest temperature of Fig. 10. Indeed, no influence of a T^{-3} dependence in C/T is evident in Fig. 10.

Low-temperature specific-heat measurements on terbium metal exhibit a large specific-heat contribution near $T \approx 0.08$ K, which can be attributed to the nuclear magnetic moment of the terbium nucleus.[35] Because the magnetic field acting on the nucleus is produced by low-lying $4f$ states, the crystalline environment should have limited effect on the energy levels.[36] Thus the specific heat observed in terbium metal may be similar to the specific heat contributed by the terbium present in our cubic zirconium. If this were true, the presence of 25 wt. ppm of terbium would dominate the specific heat near 0.2 K, contributing a temperature dependence in C/T varying roughly as $T^{-2.7}$. This dependence is not observed in Fig. 10. In addition, specific-heat measurements were performed down to a temperature of 0.08 K using a diffusive technique with a thermal-conductivity sample.[37] If terbium contributed *all* of the specific heat observed near 0.08 K, the contribution near 0.2 K of Fig. 10 would be $\approx 25\%$. However, it is more likely that the glassy excitations continue to dominate C at temperatures down to 0.08 K, and thus the terbium makes a negligible contribution to our data at $T \geq 0.2$ K. In brief, impurities are believed not to seriously distort the results shown in Fig. 10.

The specific heats of all three samples in Fig. 10 become the same above 2 K, approaching but not reaching the Debye specific heat as calculated from the sound velocities measured at room temperature.[27] At temperatures below 1.5 K, significant differences do occur. For $x=0.10$ the temperature dependence of the specific heat is linear. The magnitude of the linear term appears to scale with yttria content from $x=0.10$ to 0.16. The magnitude of a linear term for $x=0.18$ is ambiguous since the temperature dependence is less than linear.

IV. DISCUSSION OF THE RESULTS

The behavior observed for $(ZrO_2)_{1-x}(Y_2O_3)_x$ is similar to that found in amorphous solids. The specific heat, Fig. 10, is larger than that expected for Debye phonons and, below ≈ 1 K, is nearly linear in temperature. The thermal conductivity, Fig. 3, has a temperature dependence of $\approx T^2$ below 1 K. In addition, the magnitude of C or κ below 1 K is within a factor of 2—3 of the same properties in, for example, an amorphous polymer.[38] Also, the dielectric constant, Fig. 6, passes through a minimum near 0.1 K (for $\nu \approx 10^3$ Hz), and this minimum has a frequency dependence close to the $\nu^{1/3}$ dependence observed in glasses.[30]

The thermal-expansion coefficient at $T \leq 1$ K is represented by a Grüneisen parameter, Fig. 5, of $\Gamma \approx 8$, which is larger than the value $|\Gamma| \approx 2$ expected from thermal phonons. Thermal expansion is unique in that it is the one property that, although influenced or dominated by the TLS excitations found in glasses, is not universal in magnitude for all glassy solids or disordered crystals.[28]

Having established that the $(ZrO_2)_{1-x}(Y_2O_3)_x$ does exhibit low-temperature properties similar to amorphous solids, next we ask whether this behavior can be adequately explained by the AHVP tunneling-state model. The parameters of this phenomenological model must be derived from the data. Below, we present only the information needed in the computations of this section and Sec. IV.

The potential of Fig. 1 results in an energy[1] $E=(\Delta^2+\Delta_0^2)^{1/2}$ where

$$\Delta_0=\hbar\omega_0 e^{-\lambda}, \quad \lambda=(2mV_0d^2/\hbar^2)^{1/2}. \tag{4}$$

A TLS having parameters E and λ thermally relaxes with a time constant[39]

$$\tau^{-1}(E,\lambda)=\gamma^2(3/v^5)[E(\hbar\omega_0)^2/2\pi\rho\hbar^4] \times e^{-2\lambda}\coth(E/2kT), \tag{5}$$

where γ is the TLS-phonon coupling parameter, ρ is the mass density, $\hbar$ is Planck's constant divided by 2π, k is the Boltzmann constant, and v is an average phonon velocity. To explain the specific-heat data of glasses, it is required that the TLS have a broad spectrum of excitation

energies E. To obtain this broad energy density of states, the asymmetry Δ and overlap parameter λ are assumed to have a distribution $P(\Delta,\lambda)$ shown in Fig. 11 by the solid line,[40] i.e.,

$$P(\Delta,\lambda)=\begin{cases}\bar{P}, & \lambda<\lambda_{\max}\\ 0, & \lambda>\lambda_{\max}\end{cases}. \tag{6}$$

The combination of Eqs. (5) and (6) requires that the TLS exhibit a spectrum of relaxation times τ. The excess specific heat contributed by the ensemble of TLS is given by

$$C=(\pi^2k^2/6)\bar{P}\eta T\ , \tag{7}$$

where η is a weak function of the measurement period[1] and reflects the presence of the broad distribution of TLS equilibration times. Also

$$\kappa=(1/\bar{P}\gamma^2)(\rho k^3/2\pi\hbar^2)vT^2\ . \tag{8}$$

The products $\bar{P}\gamma^2$ and $\bar{P}\eta$ may be obtained from the κ and C data. The results are given in Table III for $x=0.10$ and 0.16, since these samples have $C\propto T$ below 1 K. The adoption of a value of $\eta\approx 10$, to reflect the presence of a broad spectrum of TLS relaxation times,[40] provides (for $x=0.10$) the solid lines in Figs. 3 and 10. The agreement appears satisfactory. However, the failure of this procedure to fit the time dependence of the specific-heat data is indicated in Fig. 9 for $x=0.16$. Data beyond 0.3 s are well represented by $\eta=8.7$, but at shorter times the measured "overshoot" discussed in Sec. III is much larger than that calculated from the AHVP model.

In brief, our data cannot be accounted for by the AHVP model if the model is restricted to the set of adjustable parameters which is conventionally applied. However, to account for the time dependence observed in specific-heat measurements, it has been suggested[40] that an additional set of "anomalous" TLS may be introduced which would be added to the "standard" TLS of Fig. 11. It should be noted that the anomalous TLS may be the same, microscopically, as the standard TLS. A simple example of this procedure would be to add TLS having λ centered near λ_a as shown by the dashed line in Fig. 11.

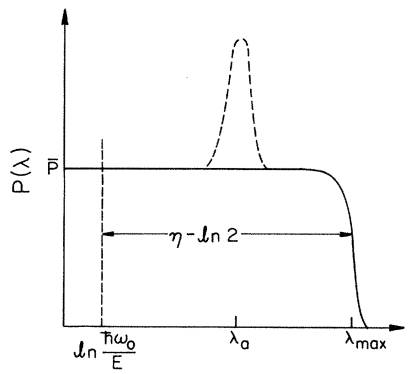

FIG. 11. Distribution in overlap parameter λ. Solid line shows standard TLS distribution. Dashed line shows anomalous TLS distribution; see text.

TABLE III. Parameters for the AHVP tunneling-state model required to fit the data. (1 D$=1.60\times10^{-29}$ Cm, and 1 erg$=10^{-7}$ J.)

Sample	$x=0.10$	$x=0.16$
$\bar{P}\gamma^2$ (erg cm^{-3})	1.2×10^{8}	1.4×10^{8}
$\bar{P}\eta$ (erg^{-1} cm^{-3})	2.3×10^{33}	3.7×10^{33}
$\bar{P}$ (erg^{-1} cm^{-3})	1.5×10^{32}	2.7×10^{32}
γ (eV)	0.56	0.44
η	11	10
$\bar{P}p_0^2$	3.8×10^{-4}	4.8×10^{-4}
p_0 (D)	0.33	0.28
$\bar{P}\eta$ (erg^{-1} cm^{-3})[a]	1.71×10^{33}	2.77×10^{33}
n_a (erg^{-1} cm^{-3})[a]	0.59×10^{33}	1.0×10^{33}
τ_aT (s K)[a]	0.031	0.018

[a] Pertains to use of anomalous TLS as discussed in the text and in Fig. 11.

The addition of this anomalous set of TLS produces the solid line of Fig. 9, which is in better agreement with the data. Figure 12 compares data and computation at two additional temperatures without changing the values of the parameters. These values (which are summarized in Table III) are not unique, but do demonstrate that the specific-heat and thermal-conductivity data on $(ZrO_2)_{1-x}(Y_2O_3)_x$ can be explained by the AHVP model. The explanation is at the expense of a greater number of adjustable parameters than was originally adopted for glassy solids, but recent measurements on real glasses encounter a similar problem.[31]

We conclude this section with two additional observations. The slopes of ϵ' versus T in Fig. 7, at temperatures

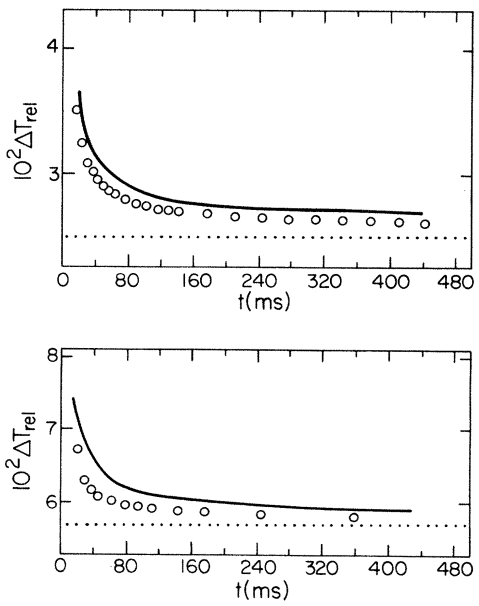

FIG. 12. Temperature overshoot as in Fig. 9, except at temperatures of 0.46 (top) and 0.68 K (bottom).

below the minimum, are proportional to $\bar{P}p_0^2$ where p_0 is the effective electric dipole moment of a TLS. Through the use of values for $\bar{P}$ deduced previously, a magnitude of $p_0=0.3$ D is obtained.

As has been discussed previously,[28,41] a γ of ≈ 0.5 eV (see Table III) for all TLS should produce a Grüneisen parameter of $\Gamma \approx 10^3$ near 1 K. The much smaller Γ of Fig. 5 can be explained if different TLS have different values of γ. The spectrum of γ might be broad and nearly centered on $\gamma=0$. The thermal conductivity measures the average of $(\gamma)^2$, which would be large, while thermal expansion measures the average of γ, which would be small.[28]

In summary, we find ZrO_2:Y_2O_3 to behave in a manner similar to an amorphous solid in its low-temperature behavior, but with a larger portion of the TLS having longer equilibration times than in most glasses. The density of states probed by the specific heat, namely $\bar{P}\eta$, is proportional to the Y_2O_3 concentration for the $x=0.10$ and 0.16 samples. As in the crystalline orientational glass KBr:KCN, the phonon mean free path remains constant as the total specific heat increases.[29] The behavior for the $x=0.18$ sample is obscured by a more complex temperature dependence of the specific heat. As mentioned in Sec. II, the $x=0.18$ sample was also less perfect in that it exhibited a yellow tinge of unknown origin. It is not understood why the $(ZrO_2)_{0.955}(Y_2O_3)_{0.045}$ ceramic sample of Ref. 6 exhibited a larger specific heat; see Fig. 10. We inquire next whether the excitations can be ascribed to a particular lattice defect.

V. MICROSCOPIC TUNNELING STATES

For the ZrO_2:Y_2O_3 system, two simple tunneling states may be present. To model these tunneling states, we use information presented in the literature concerning crystalline defects.

A double-well potential, Fig. 1, has been used to model oxygen-ion conductivity at high temperatures as well as the TLS at low temperatures for β-alumina and for ZrO_2 systems.[33,42] The barrier height[43] V_0 is given as ≈ 1 eV, and the distance between wells d is the oxygen-oxygen distance, 2.6 Å. The relaxation time for such a tunneling state can be predicted using Eq. (5). For $E \approx 0.5$ K and a reasonable attempt frequency[15] of $\omega_0 \approx 6.8\times 10^{13}$/s, an extremely long relaxation time τ is obtained. Such a tunneling state would not be observed in the present measurements.

We speculate that a second candidate for a tunneling state is the configuration of oxygen anions shown in Fig. 13, which consists of one oxygen anion in the center with two vacancies on opposite sides. This configuration will be called an "incipient" tunneling state. The rest of the nearest-neighbor oxygen sublattice sites are occupied by oxygen anions. If just one vacancy is next to the center oxygen, this oxygen collapses[12] toward the vacancy by ≈ 0.4 Å, as indicated in Fig. 2(a). With the vacancies on opposite sides, it is possible that there will be two equilibrium positions for the center oxygen due to its tendency to collapse toward both vacancies, as shown by the arrows in Fig. 13. Asymmetry will be introduced to the

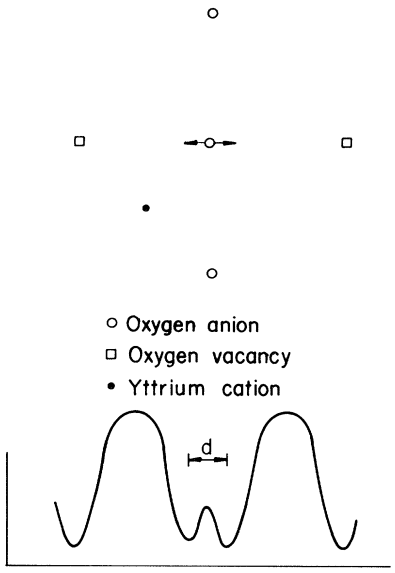

FIG. 13. Speculative microscopic model of a two-level system. The center oxygen is a possible tunneling state; a potential-energy diagram for this oxygen ion is shown at the bottom. The effective charge of the nearby yttrium cation produces an asymmetry in the double well.

double well of Fig. 13 through strain of the surrounding environment or through electrostatic interactions[9] of the oxygen with other surrounding vacancies or yttrium substitutional defects. The distance between the wells, d, is roughly twice the collapse distance giving $d \approx 0.8$ Å. The barrier height is calculated using harmonic wells separated by distance d.

The probability of an oxygen anion being an incipient tunneling state can be calculated purely statistically using the probability of finding an oxygen vacancy occupying an anion lattice site, which in turn is governed by the yttrium content. The density of incipient states computed in this way is $n_s \approx 3\times 10^{20}/\text{cm}^3$ for $x=0.16$. This value may be compared with the density deduced fom the specific-heat measurements

$$n_E=(k\ln 2)^{-1}\int_0^{T_M}(C_{\text{ex}}/T)dT\ , \tag{9}$$

where C_{ex} is the excess specific heat not associated with phonons. If the integral of Eq. (9) is limited to $T_M \leq 3$ K in Fig. 10, then $n_E \approx 3\times 10^{18}/\text{cm}^3$, which is much smaller than the statistical estimate of $n_s=3\times 10^{20}/\text{cm}^3$. Certainly, the spectrum of TLS extends to energies above 3 K, and so the difference between n_E and n_s may not be so large.[44]

The bare electric dipole moment of the incipient tunneling unit is calculated by multiplying the charge of the tunneling unit by the tunneling distance d, giving $p_{\text{inc}}=1.6$ D. This can be compared to the effective dipole moment $p_0 \approx 0.3$ D calculated from the dielectric measurements in Table III. An estimate of the bare dipole moment p may be obtained from (assuming the dipoles are randomly oriented)

$$p = 3\sqrt{3}p_0/(\epsilon+2) . \quad (10)$$

We measure $\epsilon \approx 20$, and hence $p \approx 0.07$ D, which is a factor of 20 smaller than the value of p_{inc} obtained from the statistical computation.

If the incipient tunneling states were isolated, each would have the same value for the tunneling parameter λ of Eq. (4). This value, which we will call λ_a, can be computed if the wells are assumed to be harmonic in shape, as in Fig. 1, and parametrized by published estimates[15] of ω_0 for the oxygen anions. Since some incipient tunneling states will be near impurities or other incipient states, a spread in λ will be produced through elastic and electrostatic interactions. The net result could appear as in Fig. 11. From Eq. (4) we obtain $\lambda_a \approx 50$, whereas λ_a deduced from the data in Sec. IV has the smaller value of ≈ 15. A value of d less than the assumed 0.8 Å would improve the agreement for both λ_a and the dipole moment p.

The two models we have examined for a tunneling state are both based on defects known to exist in cubic zirconia. Of the two models, the second is seen to be the most favorable. Nevertheless, the discrepancies listed above leave its applicability in doubt.

It is observed from Figs. 3 and 10 that the specific heat changes with Y_2O_3 content more than the thermal conductivity changes, yet the change in either property should be proportional to the change in density of TLS. This suggests that the TLS may not be isolated, independent defects, but may arise through interactions between those defects as appears to occur in the crystalline system KBr:KCN (Ref. 29) or in magnetic spin-glasses. If this is true, then it will be extremely difficult to model a two-level state in any disordered solid.

VI. SUMMARY

Measurements of specific heat, thermal conductivity, dielectric constant, and thermal expansion of the cubic fast-ion conductor $(ZrO_2)_{1-x}(Y_2O_3)_x$, with $x = 0.10$, 0.16, and 0.18, exhibit behavior very similar to that observed in measurements of amorphous solids and attributed to two-level states. The density of TLS appears to increase with the Y_2O_3 content. The data can be fitted by the phenomenological tunneling-state model, but require a more complex spectrum of TLS equilibration times than has generally been used for amorphous solids. Two models of a two-level state, based on defects known to exist in cubic zirconia, fail to provide satisfactory agreement with data. It is speculated that the TLS may not be associated with isolated defects.

ACKNOWLEDGMENTS

This work was supported by the Materials Sciences Division of the Department of Energy under Contract No. DE-AC02-76ER01198. One of us (F.J.W.) acknowledges the support of the Exxon Research Foundation. The authors also thank D. A. Ackerman for assistance with the thermal-expansion measurements.

[1] *Amorphous Solids: Low-Temperature Properties,* edited by W. A. Phillips (Springer, New York, 1981). We adopt the notation of this reference, except the overlap parameter Δ_0 differs in sign.

[2] P. W. Anderson, B. I. Halperin, and C. M. Varma, Philos. Mag. 25, 1 (1972).

[3] W. A. Phillips, J. Low Temp. Phys. 7, 351 (1972).

[4] V. Narayanamurti and R. O. Pohl, Rev. Mod. Phys. 42, 201 (1970).

[5] H. V. Lohneysen, H. J. Schink, W. Arnold, H. U. Beyeler, L. Pietronero, and S. Strassler, Phys. Rev. B 24, 2187 (1981).

[6] D. A. Ackerman, D. Moy, R. C. Potter, A. C. Anderson, and W. N. Lawless, Phys. Rev. B 23, 3886 (1981), and references cited therein.

[7] E. Gmelin and R. Willar, Physica (Utrecht) 108B, 1003 (1981).

[8] U. Strom, Solid State Ionics 8, 255 (1983), and references cited therein.

[9] D. B. McWhan, C. M. Varma, F. L. S. Hsu, and J. P. Remeika, Phys. Rev. B 15, 553 (1977).

[10] J. N. Dobbs, A. C. Anderson, and W. Hayes, Phys. Rev. B 28, 3559 (1983). Also, in Nasicon (Ref. 7) only a small change in excess specific heat is obtained from a large change in Na content.

[11] J. B. Cohen, M. Morinaga, and J. Faber, Jr., Solid State Ionics 3-4, 61 (1981).

[12] D. Steele and B. E. F. Fender, J. Phys. C 7, 1 (1974).

[13] A. Feinberg and C. H. Perry, J. Phys. Chem. Solids 42, 513 (1981).

[14] M. Hartmanova, Acta Phys. Slovaca 28, 188 (1978).

[15] A. S. Nowick and D. S. Park, in *Superionic Conductors,* edited by G. D. Mahan and W. L. Roth (Plenum, New York, 1976), p. 395.

[16] Obtained from Ceres Corporation, 411 Waverly Oaks Park, Waltham, MA 02154.

[17] R. P. Ingel, R. W. Rice, and D. Lewis, J. Am. Ceram. Soc. 65, C108 (1982).

[18] R. E. W. Casselton, Phys. Status Solidi A 2, 571 (1970).

[19] I. L. Chistyi, I. L. Fabelinskii, V. F. Kitaeva, V. V. Osiko, Yu. V. Pisareveskii, I. M. Sil'verstrova, and N. N. Sobolev, J. Raman Spectrosc. 6, 183 (1977).

[20] Neutron-activation studies were performed at the Institute for Environmental Studies, University of Illinois at Urbana-Champaign, Urbania, IL. 61801.

[21] P. J. Anthony and A. C. Anderson, Phys. Rev. B 19, 5310 (1979).

[22] D. A. Ackerman and A. C. Anderson, Rev. Sci. Instrum. 53, 1657 (1982).

[23] D. A. Ackerman and A. C. Anderson, Rev. Sci. Instrum. 53, 100 (1982).

[24] R. B. Stephens, Cryogenics 15, 481 (1975).

[25] M. Steinback, P. J. Anthony, and A. C. Anderson, Rev. Sci. Instrum. 49, 671 (1978).

[26] G. J. Sellers and A. C. Anderson, Rev. Sci. Instrum. 45, 1256 (1974).

[27] The longitudinal velocity is 7.7×10^3 m/s, and the transverse velocity is 4.0×10^3 m/s, for all samples (see Ref. 19). The

mass density is 5.98×10^3, 5.88×10^3, and 5.82×10^3 kg/m^3 for $x=0.10$, 0.16, and 0.18, respectively.

[28]D. A. Ackerman, A. C. Anderson, E. J. Cotts, J. N. Dobbs, W. M. MacDonald, and F. J. Walker, Phys. Rev. B 29, 966 (1984).

[29]M. Meissner, R. O. Pohl, J. M. Rowe, J. J. Rush, and S. Susman, Phys. Rev. Lett. 51, 1050 (1983); D. Moy, J. N. Dobbs, and A. C. Anderson, Phys. Rev. B 29, 2160 (1984).

[30]G. Frossati, J. de G. Gilchrist, J. C. Lasjaunias, and W. Meyer, J. Phys. C 10, L515 (1977).

[31]M. T. Loponen, R. C. Dynes, V. Narayanamurti, and J. P. Garno, Phys. Rev. B 25, 1161 (1982).

[32]W. N. Lawless, Phys. Rev. B 21, 585 (1980).

[33]W. N. Lawless, Phys. Rev. B 22, 3122 (1980).

[34]F. J. Walker, Ph.D. thesis, University of Illinois, 1983.

[35]M. Krusius, A. C. Anderson, and B. Holmstrom, Phys. Rev. 177, 910 (1969).

[36]J. E. Robichaux and A. C. Anderson, Phys. Rev. B 2, 5035 (1970).

[37]Specific-heat data obtained with the diffusive technique are not presented, as they are less quantitative than the data of Fig. 10.

[38]D. S. Matsumoto, C. L. Reynolds, and A. C. Anderson, Phys. Rev. B 19, 4277 (1979).

[39]J. Jackle, Z. Phys. 257, 212 (1972).

[40]J. L. Black, Phys. Rev. B 17, 2740 (1978).

[41]W. A. Phillips, J. Low Temp. Phys. 11, 757 (1973).

[42]W. N. Lawless and S. L. Swartz [Phys. Rev. B 28, 2125 (1983)] suggest a model which gives $\bar{P}\propto 1/x$, whereas we observe $\bar{P}\propto x$. See also W. N. Lawless and T. K. Gupta, Phys. Rev. B 28, 5507 (1983).

[43]P. Abelard and J. F. Baumard, Phys. Rev. B 26, 1005 (1982).

[44]From Fig. 10 it may be argued that, although a constant energy density of TLS may occur below an energy of 1 K, near and above 1 K the density is decreasing. This is most evident for $x=0.18$, but also appears for $x=0.10$ if one attempts to fit C with the conventional temperature dependence $AT+BT^3$.